The Astrophysical Journal, 936:63 (7pp), 2022 September 1 https://doi.org/10.3847/1538-4357/ac82b7

Modeling Long-term Variability in Stellar-compact Object Binary Systems for Mass Determinations

Nicholas M. Sorabella[1,2], Sayantan Bhattacharya[1,2], Silas G. T. Laycock[1,2], Dimitris M. Christodoulou[1,3], and Alessandro Massarotti[4,5]
[1] Lowell Center for Space Science and Technology, Lowell, MA 01854, USA; nicholas_sorabella@student.uml.edu
[2] Department of Physics and Applied Physics, University of Massachusetts Lowell, Lowell, MA 01854, USA
[3] Department of Mathematical Sciences, University of Massachusetts Lowell, Lowell, MA 01854, USA
[4] Harvard-Smithsonian Center for Astrophysics, 60 Garden Street, Cambridge, MA 02138, USA
[5] Department of Physics and Astronomy, Stonehill College, 320 Washington Street, Easton, MA 02357, USA
Received 2022 May 11; revised 2022 July 7; accepted 2022 July 18; published 2022 August 31

Abstract

This work models the effects of gravitational lensing, Doppler boosting, and ellipsoidal variations on eccentric eclipsing binary-system light curves. This is accomplished using a Newtonian orbital-motion code that simulates the orbital velocities and separation of the binary components as a function of time. Improving on previous literature, we examine the effects of orbital eccentricity and period, as well as stellar limb darkening on the expected light curves. Whether lensing, Doppler boosting, or ellipsoidal variation is dominant in the light curves is a function of the separation between the binary components; thus, the combination of all three effects allows for a unique mass-determination method that greatly expands the parameter space for the discovery of compact objects. This suggests the exciting possibility of revealing a large population of nonaccreting compact objects in galactic binary systems. At the same time, the model can be used on systems exhibiting any subset of these effects. In a case study, we fit our model to optical data from the ellipsoidal variable binary system Cygnus X-1, and we compare our determinations with those previously found by different modeling techniques.

Unified Astronomy Thesaurus concepts: Black hole physics (159); Compact binary stars (283); Ellipsoidal variable stars (455); Gravitational microlensing (672)

1. Introduction

It was in Trimble & Thorne (1969) where the idea to use gravitational lensing to measure the mass of a compact object in an eclipsing binary was first postulated. As described in Maeder (1973), the compact object (white dwarf, neutron star, or black hole) will vary the apparent luminosity of its stellar companion as it eclipses the star from our line of sight. As seen in Figure 1, a gravitational lens increases the apparent surface area of a star behind it, making the star appear brighter to a distant observer. A lensing event in a binary system has been given the term "self-lensing" and, given that the two objects orbit one another, self-lensing signals are periodic, appearing once per orbit.

Increases in luminosity of a star, as caused by gravitational lensing, have been observed in the so-called "microlensing" events, where a compact object serendipitously passes between our line of sight and a more distant star (e.g., Alcock et al. 1993). The magnification caused by a lensing event is proportional to the distance between the lens and the object being magnified (referred to as the source). Hence, these microlensing events can produce very large changes in the source's apparent magnitude due to the extreme distances between the two objects. In contrast, a compact object in a binary system is extraordinarily close to its source by astronomical standards, meaning the expected magnification will be much smaller, on the order of a millimagnitude. For this reason, the discovery of self-lensing signals has proven to be quite difficult.

Modeling of expected self-lensing pulses was conducted by Witt & Mao (1994), Marsh (2001), and Rahvar et al. (2011). Witt & Mao (1994) created a mathematical description for the lensing of an extended source, i.e., a source that has a defined size relative to the lens (note that most microlensing events to date use point-source approximations). Marsh (2001) focused attention on self-lensing events where the compact object is a white dwarf (WD) star and Rahvar et al. (2011) created a model specific to lensing of main-sequence stars. It was not until Kruse & Agol (2014), 45 yr after the concept of self-lensing was first described, that the first self-lensing event was discovered by the Kepler Space Telescope. The Quasiperiodic Automated Transit search algorithm discovered a series of periodic increases in brightness from the star system KOI-3278 (Kruse & Agol 2014). The amplification was only a factor of 1.001 times the nonlensed flux, a relatively small increase, yet a significant detection in the Kepler data. From this increase in brightness, together with the duration and the profile of the feature, Kruse & Agol (2014) inferred that the object was a WD star of $0.63^{+0.047}_{-0.055}$ solar masses. Since then, additional self-lensing discoveries have been found in the same vein; all five stellar-mass self-lensing systems discovered so far were found in Kepler data, and consisted of a WD eclipsing its sunlike companion star (Masuda et al. 2019).

Masuda & Hotokezaka (2019) went further in their modeling effort, including not only self-lensing but also additional dynamical effects expected in a binary system containing a compact object. Doppler boosting produces a modulation in the light curve of the system, with the amplitude of the effect determined primarily by the radial velocity of the companion

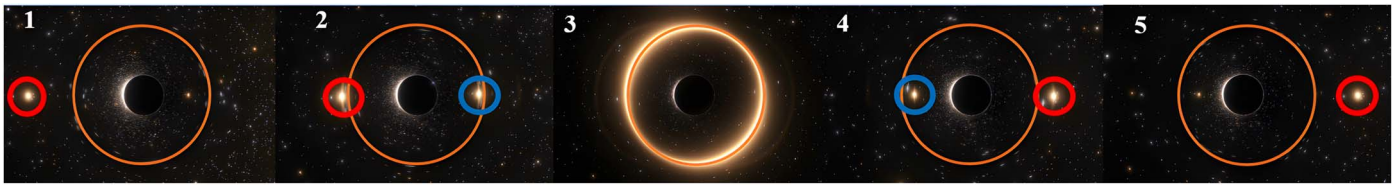

Figure 1. A step-by-step process of a black hole gravitationally lensing a background star. Panel 1 shows the star (circled in red) just outside the Einstein radius (orange). Panel 2 shows the surface area of the star increasing as a secondary image of the star (circled in blue) forms. Panel 3 depicts when the black hole is directly in front of the star; the two images of the stars connect to form a perfect ring around the black hole where maximum amplification occurs. Panel 4 shows the image of the star returning to normal, as the secondary image begins to fade. Finally, panel 5 shows the lensing process having been completed. This figure was created using SpaceEngine.[6]

star and the overall shape dependent on the eccentricity and argument of periapsis (D'Orazio et al. 2015). Ellipsoidal variations are created by the extreme tidal forces between the compact object and its stellar companion, distorting the star into a teardrop shape (Morris 1985; Beech 1986). These effects, combined with self-lensing, are particularly useful given that both ellipsoidal variations and Doppler boosting are strongest in systems with short orbital periods (and smaller separations), whereas self-lensing is strongest in systems with longer orbital periods. This combination effectively expands the parameter space not only for discovering compact objects in binary systems, but also for determining their masses.

In this work, we have gone a step further in modeling these types of systems by including the effects of stellar limb darkening on the self-lensing pulse, as well as eccentric binary orbits on the resulting light curve. Our modeling produces synthetic light curves with distinct shapes that can be used to determine characteristics of the binary components such as component masses, as well as the orbital inclination, eccentricity, and the stellar radius. We describe our Newtonian orbital-motion code in Section 2, and the mathematical model for self-lensing, Doppler boosting, and ellipsoidal variations in Sections 3–5, respectively. We illustrate the overall light curve resulting from the combination of all three effects in Section 6. In Section 7, we investigate the possibility of self-lensing in binaries containing millisecond pulsars with WD companions, as well as black-widow binaries. We discuss the importance of modeling all three effects in Section 8 and we apply the model to a light curve of Cygnus X-1 in order to independently determine the binary parameters of this system. Finally, our results and conclusions are summarized in Section 9.

2. Modeling Binary Star Orbits

In order to model the light curve of a binary star system that undergoes effects such as self-lensing, Doppler boosting, and ellipsoidal variations, one needs to be able to keep track of the binary-component relative velocities and the orbital separation as a function of time. For circular orbits, this is not difficult, given that the orbital velocities and the binary separation remain constant in magnitude throughout the orbit. However, we want our model to be applicable to eccentric binary systems as well, in which case these parameters will be variable. With this in mind, we developed a numerical code in Mathematica that uses a system of differential equations derived from Newtonian mechanics to model the eccentric orbits of the compact object and its companion star. This is similar to the method described in Sorabella et al. (2022) with the exception that we have replaced the Paczysnki–Wiita potential with the classical Newtonian potential. Four differential equations are used to keep track of the binary component positions and accelerations in Cartesian coordinates as a function of time, viz.

$$x_1''(t) = -\frac{Gm_1m_2(x_1(t) - x_2(t))}{m_1((x_1(t) - x_2(t))^2 + (y_1(t) - y_2(t))^2)^{3/2}}, \quad (1)$$

$$y_1''(t) = -\frac{Gm_1m_2(y_1(t) - y_2(t))}{m_1((x_1(t) - x_2(t))^2 + (y_1(t) - y_2(t))^2)^{3/2}}, \quad (2)$$

$$x_2''(t) = \frac{Gm_1m_2(x_1(t) - x_2(t))}{m_2((x_1(t) - x_2(t))^2 + (y_1(t) - y_2(t))^2)^{3/2}}, \quad (3)$$

$$y_2''(t) = \frac{Gm_1m_2(y_1(t) - y_2(t))}{m_2((x_1(t) - x_2(t))^2 + (y_1(t) - y_2(t))^2)^{3/2}}. \quad (4)$$

The double-primed variables are the accelerations in the x and y directions of the compact object and the companion star (labeled 1 and 2, respectively), and the unprimed variables represent their positions. This system of differential equations is solved using Mathematica's built-in numerical differential equation solver called `NDSolveValue`, which returns four interpolating functions that allows one to track the motions of the components as a function of time. An example binary system containing a sunlike star and a $10\,M_\odot$ black hole is shown in Figure 2.

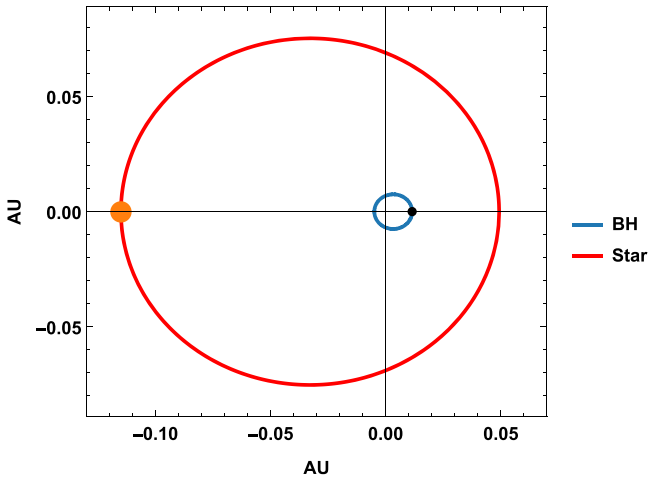

Figure 2. The orbits of a sunlike star and a $10\,M_\odot$ black hole. The orbital period is 3 days and the eccentricity is set to $e = 0.3$. The black hole size is exaggerated, so it can easily be seen, but the size of the star is to scale relative to the size of its orbit. The origin of the coordinate system is the center of mass of the binary.

3. Self-lensing Theory

The two primary variables needed to calculate the amplitude and the duration of a self-lensing pulse are the angular

[6] http://spaceengine.org/

separation $u(t)$ and the ratio between the source radius and the so-called Einstein radius, $P_\star$. The Einstein radius is the effective radius of the lensing effect, and it is given by the equation

$$R_{\rm E} = \sqrt{\frac{4GMd(t)}{c^2}}, \tag{5}$$

where G is the gravitational constant, M is the mass of the lens, $d(t)$ is the separation between the binary components, and c is the speed of light. The orbital separation $d(t)$ is found using the position vectors of the two components.

One can compute the angular separation $u(t)$ in terms of the Einstein radius as a function of time from the equation

$$u(t) = \sqrt{u_0^2 + \left(\frac{t - t_0}{t_{\rm E}}\right)^2}, \tag{6}$$

given that

$$u_0 = \frac{d(t)}{R_{\rm E}}\psi, \tag{7}$$

is the closest angular approach during the eclipse and angle ψ is the inclination of the source relative to the observer-lens line of sight. The parameter $t_{\rm E}$ in Equation (6) represents the Einstein time, the time it takes for the lens to move across the length of its Einstein radius $R_{\rm E}$.

The ratio of the source size to the size of the lens is denoted by $P_\star$. In our case, the source size corresponds to the radius of the companion star $R_\star$, in which case

$$P_\star = \frac{R_\star}{R_{\rm E}}. \tag{8}$$

Continuing, one can substitute the values of $u(t)$ and $P_\star$ into the equation for amplification as a function of time (Hamolli et al. 2015), viz.

$$A = \frac{\int_0^{2\pi}\int_0^{P_\star}\left(\frac{\xi^2+2}{\xi\sqrt{\xi^2+4}}\right)S\ r dr d\theta}{2\pi\int_0^{P_\star} S\ r dr}, \tag{9}$$

where

$$\xi^2 = u^2 + r^2 - 2ur\cos\theta, \tag{10}$$

and the variable $S(r)$ represents the brightness profile of the source. We chose to model the brightness profile using the linear limb-darkening relation of Hamolli et al. (2015) and Han (2016), viz.

$$S(r) = 1 - \Gamma\left[1 - \frac{3}{2}\sqrt{1 - \left(\frac{r}{P_\star}\right)^2}\ \right]. \tag{11}$$

The term Γ represents the limb-darkening coefficient, where $\Gamma = 0$ corresponds to a source with constant surface brightness. As Γ increases, so does the limb darkening of the source star.

The double integral in Equation (9) cannot be solved analytically. Instead, we use the method of Gaussian quadrature to approximate the integral numerically. We display the results of the numerical quadrature in Figure 3. Limb darkening results in an increase of the maximum amplification observed, as well as more rounded pulses. Including limb darkening helps to better constrain the mass of the compact object and the physical parameters of the stellar companion, given that it is directly tied to the stellar temperature.

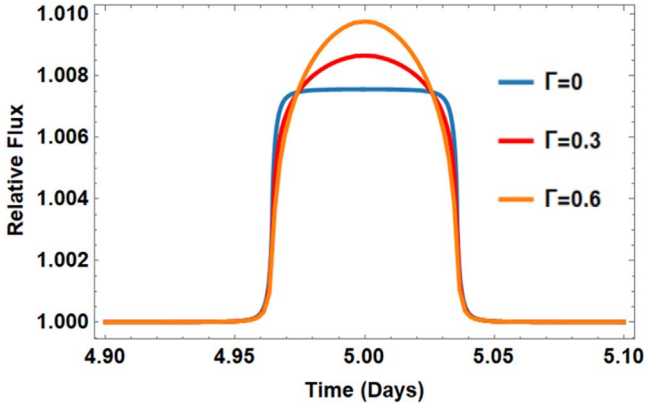

Figure 3. The self-lensing pulses of stellar sources with various limb-darkening coefficients. For the compact object, the model assumes a black hole of 10 $M_\odot$ and an orbital period of 10 days. The stellar companion has a mass of 2 $M_\odot$ and a radius of 1 $R_\odot$. The system is viewed edge on ($\psi = 0°$). Note that an increase in Γ results in an increase in amplification and a more rounded pulse.

4. Doppler Boosting

With the finite source self-lensing aspect of the modeling accounted for, we turn to the Doppler-boosting component of the model. Doppler boosting is a change of the binary system brightness as the stellar companion moves toward or away from the observer along its orbit. For the observed flux $F_\nu \propto \nu^\alpha$, we adopt the Doppler-boosting amplitude given by D'Orazio et al. (2015) and Hu et al. (2020), viz.

$$\frac{\Delta F_\nu}{F_\nu} = \pm(3 - \alpha)(v/c)\cos\phi\sin i, \tag{12}$$

where α is the average spectral index over the observed band, v is the radial velocity of the companion star, ϕ is the orbital phase, and $i = 90° - \psi$ is the orbital inclination. The radial velocity depends on the star's line-of-sight vector, which depends on the eccentricity, inclination, and argument of periapsis of the binary system.

We note that at a specific frequency ν, $\alpha(\nu)$ can be calculated from the observed spectrum (Loeb & Gaudi 2003; van Kerkwijk et al. 2010; Shporer 2017). Assuming that the stellar source is a blackbody, one finds that

$$\alpha(\nu) = \frac{e^x(3 - x) - 3}{e^x - 1}, \tag{13}$$

where $x = h\nu/(kT_{\rm eff})$, h is Planck's constant, k is Boltzmann's constant, and $T_{\rm eff}$ is the effective temperature of the source. Then, since $\nu \propto 1 + v/c$, the observed flux is $F_\nu \propto 1 + (3 - \alpha)v/c$ (Loeb & Gaudi 2003).

5. Ellipsoidal Variations

It is expected that, in particularly close binary systems, tidal forces between the compact object and its companion star will result in ellipsoidal variations in the systems' light curve. The amplitude of this effect is given by the equation described in Morris & Naftilan (1993) and Masuda & Hotokezaka (2019),

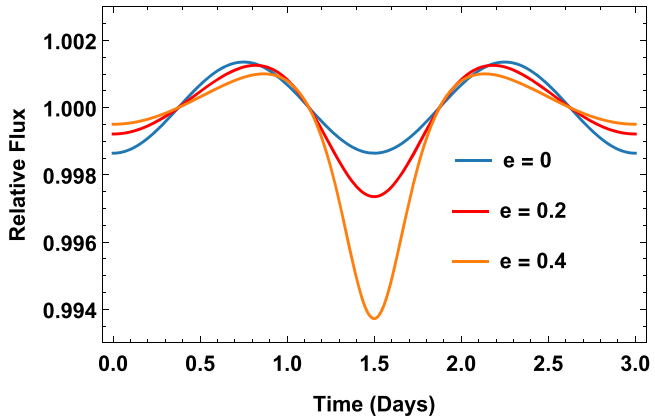

Figure 4. The effect of ellipsoidal variations on a light curve of a binary system containing a sunlike star and a $10\,M_\odot$ black hole. The orbital period is 3 days, the orbital inclination is $i = 90°$, $\beta = 1$, and the argument of periapsis ω is set to 90°. As the eccentricity of the system increases, the amplitude of the change in flux increases at periapsis, whereas it slightly decreases at apoapsis.

viz.

$$s_{\rm ev} = \beta \frac{M}{M_\star}\left(\frac{R_\star}{d}\right)^3 \sin^2 i, \tag{14}$$

where M is the mass of the compact object, $M_\star$ is the mass of the companion star, d is the separation between the two objects, $R_\star$ is the radius of the star, and i is the inclination of the orbit. The coefficient β is a function of the limb-darkening and gravity-darkening coefficients (Γ and g, respectively), viz.

$$\beta = 0.15(1+g)\frac{15+\Gamma}{3-\Gamma}. \tag{15}$$

Figure 4 shows the effect of eccentricity on the shape of the light curve of a binary system displaying ellipsoidal variations. As in Figure 2, we assume a sunlike star with a $10\,M_\odot$ black hole companion and an orbital period of 3 days. We also assume that the orbital inclination is $i = 90°$, $\beta = 1$, and the argument of periapsis ω is set to 90°. This ω value corresponds to the black hole eclipsing the star at periapsis ($t = 1.5$ days) with the opposite occurring at apoapsis ($t = 0$ and $t = 3$ days). For a circular orbit ($e = 0$), the amplitude of the flux variation remains the same at ± 0.0014. As the eccentricity increases, a much larger flux variation occurs when the binary components are at periapsis, where the tidal forces between the two components are the strongest. On the other hand, a small decrease in flux variation occurs at apoapsis, where the tidal forces are weakest because of the increased separation of the components.

6. All Effects Combined

With self-lensing, Doppler boosting, and ellipsoidal variations accounted for, we examine how their combination changes the overall shape of the light curve. Considering all three effects, the overall magnification is given by the equation

$$1 + \Delta F_{\rm tot} = A\left(1 + \left(s_{\rm ev} + \frac{\Delta F_\nu}{F_\nu}\right)\right), \tag{16}$$

where A is the amplification caused by self-lensing (Equation (9)), $s_{\rm ev}$ is the amplitude of the change in flux caused by ellipsoidal variations (Equation (14)), and $\frac{\Delta F_\nu}{F_\nu}$ is the amplitude change due to Doppler boosting (Equation (12)).

We have plotted the light curves of an example binary system in Figure 5, where we assumed one case with circular orbits (left) and another in which $e = 0.3$ (right). Individual contributions to the relative flux are plotted by dashed lines, and the total light curve is shown in solid purple. We note that the left plot is virtually identical to the corresponding figure in Masuda & Hotokezaka (2019), where they assumed the exact same conditions. This confirms that our self-lensing model with Doppler boosting reproduces the results obtained in published literature. On the right plot, we see an entirely new result—the effect of nonzero eccentricity on the shape of the model light curve. The slope of the Doppler-boosting curve is steeper, the timescale of the self-lensing event is slightly shorter, and the height of the pulse is also shorter.

What effect contributes the greatest change in flux depends on the separation between the compact object and its companion star. Figure 6 demonstrates how the peak amplification, as caused by each effect, varies as we increase the orbital period of the binary, thus increasing the binary separation. In this example system (a $10\,M_\odot$ black hole and a sunlike companion), ellipsoidal variations would produce the greatest change in flux for orbital periods of <2 days. Doppler boosting is the dominant effect for periods of 2–5 days, and self-lensing becomes entirely dominant for periods >5 days. Ellipsoidal variations and Doppler boosting both decrease with increasing separation, albeit at different rates; the change in flux caused by ellipsoidal variations drops much faster with orbital period than the change in flux due to Doppler boosting. At the same time, the amplification due to self-lensing actually increases with separation, and this element proves to be particularly useful in constraining the binary parameters when fitting the model to observed light curves. For example, if such a binary system had an orbital period of 10 days and no self-lensing event, we can deduce that it is not eclipsing, which further constrains its orbital inclination.

7. White Dwarfs, Black Widows, and Inclination Effects

The recent discovery of PSR J0740+6620, one of the most massive pulsars yet found (Cromartie et al. 2020), provides another prospect for self-lensing events. With a mass of $2.14\,M_\odot$, a WD companion mass of $0.260\,M_\odot$, a WD radius of $\approx 0.02\,R_\odot$, and an orbital period of 4.7669 days (Cromartie et al. 2020), PSR J0740+6620 would produce a maximum amplification of 1.9728 times its unlensed flux at $i = 90°$, significantly larger than any previous self-lensing event ever detected. However, the estimated inclination through the Shapiro delay is $i = 87.^\circ38$, and for the measured orbital period, this system cannot produce a self-lensing event. This is due to of the extremely small angular size of the WD companion. The inclination would have to be $i > 89.^\circ88$ to produce such a large relative flux increase, and $i > 89.^\circ38$ for an increase similar to the detected WD and main-sequence star self-lensing signals. However, by predicting the theoretical amplification expected from such a self-lensing event, the lack of signal would help us further constrain the inclination of such a system.

Marsh (2001) mentions the possibility of measuring self-lensing in systems containing millisecond pulsars with WD companions. We agree that self-lensing in these systems would produce large flux increases, although the size of the

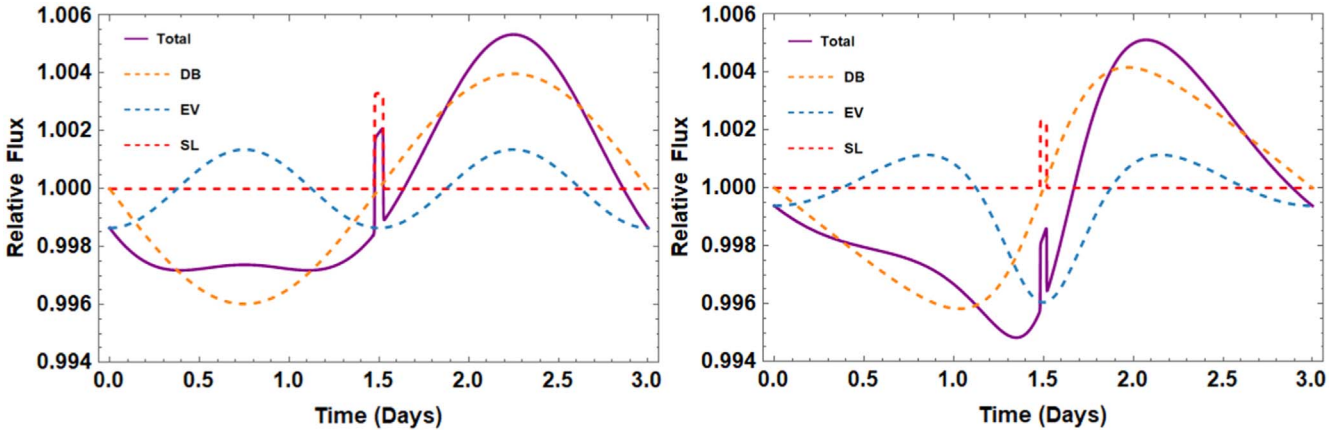

Figure 5. The light curves for an example binary system of a sunlike star and a 10 $M_\odot$ black hole with a 3 day orbital period. Doppler boosting is plotted in orange, ellipsoidal variations in blue, self-lensing in red, and the overall light curve in purple. On the left, we have assumed circular orbits. On the right, we see how the shape of each effect and the overall light curve change for an eccentricity of $e = 0.3$.

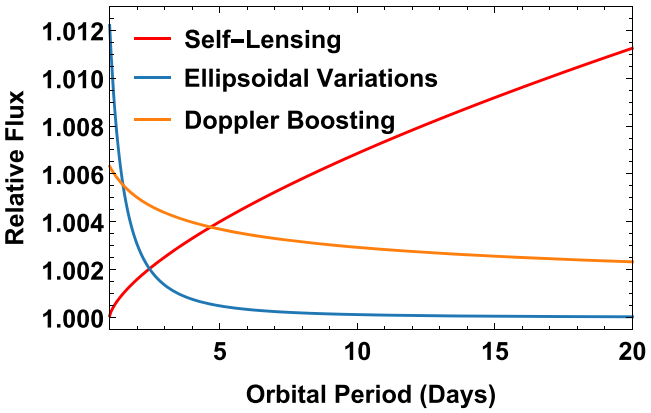

Figure 6. The maximum amplification as caused by self-lensing, ellipsoidal variations, and Doppler boosting as a function of orbital period in an example binary system. We assume that the binary is composed of a sunlike star and a black hole of 10 $M_\odot$ in circular orbits.

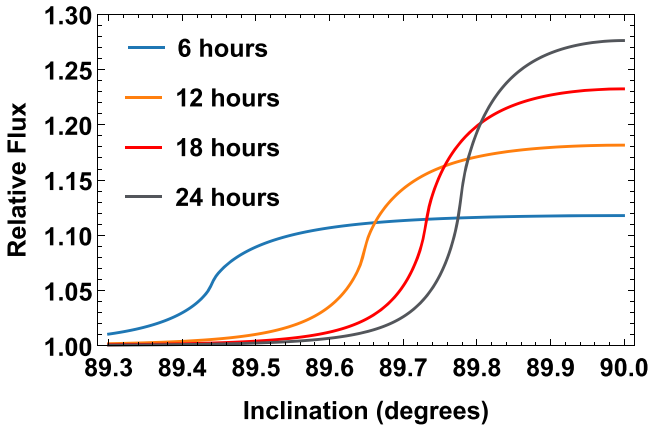

Figure 7. The maximum amplifications produced by a neutron star eclipsing a WD companion as a function of inclination angle for a variety of different orbital periods. We assume a neutron star mass of 1.44 $M_\odot$, a WD mass of 0.4 $M_\odot$, and a WD radius of 0.02 $R_\odot$. We can see that high inclination angles are needed for self-lensing to be observable. Also, shorter orbital periods produce smaller flux increases, but they allow for a greater range of inclination angles that can create an observable self-lensing event.

companion would make a proper alignment extremely rare. We have examined this relation between the inclination and the amplification more closely. Figure 7 shows the maximum amplifications produced in such systems as a function of the inclination for a variety of different orbital periods. What we find is that, while longer orbital periods allow for higher possible flux increases, the range of inclination angles where this is true is far smaller than that of shorter orbital periods. While an 18 hr orbital period would produce a flux increase similar to that of KOI-3278 (Kruse & Agol 2014) at $i = 89.^\circ4$, a 6 hr orbit would require only $i = 89^\circ$ to produce a similar change in flux.

We would also like to add the possibility of detecting self-lensing in so-called "black-widow" binaries. As an example, PSR B1957+20 is the ubiquitous "Black Widow Pulsar," and it is orbited by a degenerate hydrogen core with a mass of only 0.024 $M_\odot$ and a radius of 0.16 $R_\odot$, that undergoes eclipses every 9.2 hr (Djorgovski & Evans 1988). The flux increase in this configuration would be 1.00276 times the unlensed flux at $i = 90^\circ$, which is a bit higher than what was observed with all known stellar-mass self-lensing systems. However, in the case of PSR B1957+20, the eclipses it experiences are not those of the companion passing in front of the pulsar. Instead, a wind of material being ablated off the companion by the radiation pressure of the pulsar appears to be the cause of the eclipses, blocking the light from the pulsar once per orbit.

We examined the minimum required orbital inclination for a self-lensing pulse in Figure 8 for three kinds of systems as a function of orbital period: neutron star (NS)–WD binaries, black widow binaries and main-sequence (MS)–black hole (BH) binaries. For simplicity, we assume circular orbits for these cases. To find the minimum acceptable inclination $i_{\rm min}$, we adopt the methodology of Wiktorowicz et al. (2021); for the maximum impact parameter, the minimum inclination is determined by the equation $i_{\rm min} = \arccos\left(\frac{R_E + R_\star}{d}\right)$, where d is the orbital separation between the lens and the source at mid-eclipse. The NS–WD binary assumes a NS mass of 1.44 $M_\odot$, a WD mass of 0.4 $M_\odot$, and a WD radius of 0.02 $R_\odot$. The black widow binary assumes a NS mass of 1.60 $M_\odot$, a degenerate core mass of 0.024 $M_\odot$, and a radius of 0.16 $R_\odot$. The MS–BH system assumes a sunlike star and a 10 $M_\odot$ BH. As expected, NS–WD binaries require the highest minimum inclination for a self-lensing pulse due to the small angular size of the WD source. As the orbital period increases, thus decreasing the angular size of the source relative to the angular size of the

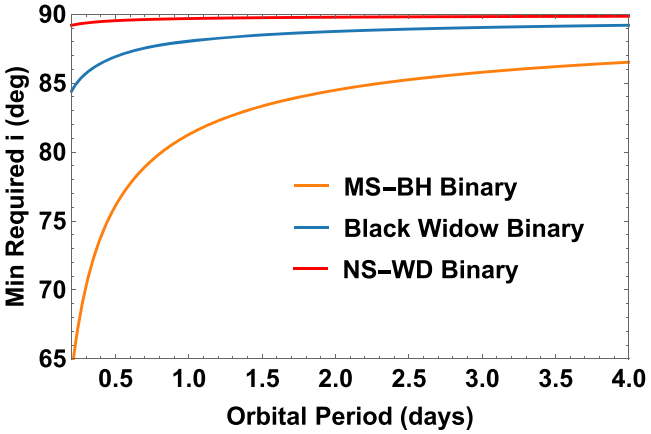

Figure 8. The minimum required orbital inclination to produce a self-lensing pulse for a MS–BH binary, a black widow binary and a NS–WD binary. The largest minimum angle required would be for the NS–WD system as the WD source has a far smaller angular size relative to the MS and the degenerate core counterparts.

lens, the minimum inclination angle increases, requiring a near-perfect alignment ($i \approx 90°$) for a substantial lensing signal to occur.

As mentioned in King et al. (2005), all black widow binaries discovered so far have orbital periods < 10 hr. Referring again to Figure 8, black widow binaries at these orbital periods have a range of available inclinations that would result in self-lensing pulses, increasing the probability for proper alignment. King et al. (2005) also suggested that the number of black widow binaries is comparable to the population of isolated millisecond pulsars. According to Chen et al. (2013), there are roughly 300 millisecond pulsars discovered in our Galactic field and the globular clusters. Assuming a uniform distribution of inclination angles ranging from 0° to 90°, it is likely that, given a similar number of black widow binaries, at least one will have the proper alignment for a measurable self-lensing pulse.

8. Discussion

Recent population synthesis studies by Wiktorowicz et al. (2021) have estimated the amount of self-lensing systems that will be observed by upcoming surveys such as LSST, TESS, and Zwicky Transient Facility to be of the order of 10^3–10^4. A large fraction of these systems will undergo self-lensing events that would result in amplifications smaller than a millimagnitude difference, thus, the pulses would be indistinguishable from noise. However, Wiktorowicz et al. (2021) estimate up to 200 of such systems that will create self-lensing pulses that will be detectable and distinguishable by the surveys. This would put the amount of discovered self-lensing systems on the same order as that of known X-ray binary (XRB) systems. These systems will likely have little to no interaction between the compact object and the companion star, completely distinct from the XRB systems. As there have been only five stellar-mass self-lensing systems observed so far, there are still many more such systems to be observed in the decades to come. As shown by Masuda & Hotokezaka (2019), a significant fraction of these systems will exhibit additional dynamical and photometric effects, such as our studied Doppler boosting and ellipsoidal variations. Thus, our model, which incorporates all three of these effects, will prove useful in future studies, as more observational data will be collected.

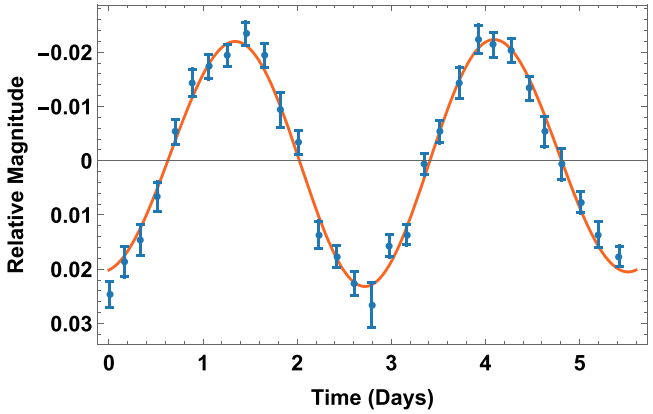

Figure 9. Optical data from Cygnus X-1 with our best-fit model denoted by the orange curve. This model assumes an orbital period of 5.59 days and argument of periapsis of $\omega = 306.^{\circ}6$, as found by Miller-Jones et al. (2021). Our best-fit parameters are listed in Table 1, along with the best-fit values determined by Miller-Jones et al. (2021).

Table 1
Cygnus X-1 Best-fit Parameters

Parameter	This Paper	Miller-Jones et al. (2021)
Black Hole Mass ($M_{\odot}$)	21.31 ± 0.10	$21.2^{+2.2}_{-2.3}$
Companion Star Mass ($M_{\odot}$)	40.30 ± 1.73	$40.6^{+7.7}_{-7.1}$
Stellar Radius ($R_{\odot}$)	27.14 ± 0.78	$22.3^{+1.8}_{-1.7}$
Eccentricity	0.029 ± 0.003	$0.0189^{+0.0028}_{-0.0026}$
Orbital Inclination (deg)	28.08 ± 1.38	$27.51^{+0.77}_{-0.57}$
True Anomaly (deg)	58.73 ± 0.04	
Average Spectral Index	1.05 ± 0.23	
Correlation R^2	0.983	
Reduced χ^2	1.049	

Our model combines the effects of self-lensing, Doppler boosting, and ellipsoidal variations into one equation (Equation (16)). It is worth noting that this model can be used to investigate any system that might exhibit any one of these effects and any combination thereof. As a particular example, we have fitted the model using Mathematica's built-in `NonLinearModelFit` function to optical data from the X-ray binary system Cygnus X-1 (Kemp et al. 1987), and the results are shown in Figure 9. We adopted an orbital period of 5.59 days and an argument of periapsis of $\omega = 306.^{\circ}6$, as found by Miller-Jones et al. (2021). We also adopted $\Gamma = 0.4$ and $g = 0.4$, the values found by Becker et al. (1978) and Guinan et al. (1979) to be optimum for O9.7 stars such as the host star in Cygnus X-1. We varied our Γ and g values within the accepted O-star range of 0.3–0.5, but this did not produce better statistical fits to the observed light curve.

At an inclination of about 28° (Table 1), Cygnus X-1 is not an eclipsing binary, thus a self-lensing event cannot occur. Furthermore, Doppler boosting contributes very little to the light curve, meaning the observed signal stems primarily from the strong ellipsoidal variations caused by the tidal gravitational field of the companion black hole. Our model accounts for the lack of self-lensing pulses and for the small Doppler-boosting contribution during fitting of the observed data, helping to rule out certain binary orientations and component mass combinations.

We determined the masses of the two components, the radius of the stellar companion, the orbital inclination, eccentricity,

and the true anomaly of the binary. The resulting best-fit parameters are listed in Table 1, along with recently published best-fit values obtained by a different method. Our best-fit model returned an R^2 value of 0.983, a $\chi^2 = 24.13$ (for 23 degrees of freedom), a reduced $\chi^2 = 1.049$, and a p-value of 0.3969, suggesting no statistically significant difference between our model and the data. The error bars were calculated assuming a 68% confidence interval for both our model and the Miller-Jones et al. (2021) model.

Nearly all of the parameters returned by our model were within the error bars shown in Miller-Jones et al. (2021), who utilized a markedly different methodology in determining the binary parameters. Their model does not take into consideration limb-darkening or gravity-darkening coefficients, whereas our model is dependent on these values. Furthermore, their model depends on the distance to the binary system, while our model is independent of the distance. The only parameters that we found to have a statistically significant difference ($>1\sigma$) from that of the Miller-Jones et al. (2021) model were the stellar radius and eccentricity (though both eccentricities suggest a near circular orbit). Our estimated radial velocity semiamplitude of 77.1 km s^{-1} from our binary parameters fits well within the spectroscopic data reported in Miller-Jones et al. (2021; see Figure S10 of their paper). Regardless, both models agree that Cygnus X-1 is among the most massive black holes ever found in an X-ray binary system.

9. Conclusions

We have modeled the effects of self-lensing, Doppler boosting, and ellipsoidal variation in eclipsing binary systems using our Newtonian orbital-motion code. We have built upon the previous work of Masuda & Hotokezaka (2019) by including the effects of stellar limb darkening on the self-lensing signal, as well as the eccentric binary orbits. We examined how eccentricity changes the profile of each effect separately, as well as the shape of the overall light curve. We have also examined the effect orbital period has on the amplitude of each signal, demonstrating that as the separation between the binary components increases, so too does the effect of self-lensing, whereas the other two effects diminish considerably.

We have discussed the potential for self-lensing in WD–NS and black widow binary systems, including the range of inclination angles for which the signal would be detectable. As a demonstration of the versatility of the model in determining binary parameters, we have fitted optical data from Cygnus X-1, an X-ray binary system known to exhibit ellipsoidal variations and a small degree of Doppler boosting. Our best-fit parameters (Table 1) are consistent with those determined by Miller-Jones et al. (2021), even though our models are not dependent on all of the same parameters. As the population of discovered self-lensing systems increases in the future, a model including all three effects will help better determine the orbital parameters and masses of the binary components.

ORCID iDs

Nicholas M. Sorabella https://orcid.org/0000-0002-3562-9699
Sayantan Bhattacharya https://orcid.org/0000-0001-8572-8241
Silas G. T. Laycock https://orcid.org/0000-0002-8427-0766
Dimitris M. Christodoulou https://orcid.org/0000-0002-7652-2206

References

Alcock, C., Akerlof, C. W., Allsman, R. A., et al. 1993, Natur, 365, 621
Becker, R. S., Bolland, T. K., & Shieh, S. Y. 1978, ApJ, 222, 647
Beech, M. 1986, Ap&SS, 125, 69
Chen, H.-L., Chen, X., Tauris, T. M., & Han, Z. 2013, ApJ, 775, 27
Cromartie, H. T., Fonseca, E., Ransom, S. M., et al. 2020, NatAs, 4, 72
Djorgovski, S., & Evans, C. R. 1988, ApJL, 335, L61
D'Orazio, D. J., Haiman, Z., & Schiminovich, D. 2015, Natur, 525, 351
Guinan, E. F., Dorren, J. D., Siah, M. J., & Koch, R. H. 1979, ApJ, 229, 296
Hamolli, L., Hafizi, M., De Paolis, F., & Nucita, A. A. 2015, AdAst, 2015, 402303
Han, C. 2016, ApJ, 820, 53
Hu, B. X., D'Orazio, D. J., Haiman, Z., et al. 2020, MNRAS, 495, 4061
Kemp, J. C., Karitskaya, E. A., Kumsiashvili, M. I., et al. 1987, SvA, 31, 170
King, A. R., Beer, M. E., Rolfe, D. J., Schenker, K., & Skipp, J. M. 2005, MNRAS, 358, 1501
Kruse, E., & Agol, E. 2014, Sci, 344, 275
Loeb, A., & Gaudi, B. S. 2003, ApJ, 588, L117
Maeder, A. 1973, A&A, 26, 215
Marsh, T. R. 2001, MNRAS, 324, 547
Masuda, K., & Hotokezaka, K. 2019, ApJ, 883, 169
Masuda, K., Kawahara, H., Latham, D. W., et al. 2019, ApJL, 881, L3
Miller-Jones, J. C. A., Bahramian, A., Orosz, J. A., et al. 2021, Sci, 371, 1046
Morris, S. L. 1985, ApJ, 295, 143
Morris, S. L., & Naftilan, S. A. 1993, ApJ, 419, 344
Rahvar, S., Mehrabi, A., & Dominik, M. 2011, MNRAS, 410, 912
Shporer, A. 2017, PASP, 129, 072001
Sorabella, N. M., Bhattacharya, S., Laycock, S. G. T., Christodoulou, D. M., & Massarotti, A. 2022, ApJ, 927, 234
Trimble, V. L., & Thorne, K. S. 1969, ApJ, 156, 1013
van Kerkwijk, M. H., Rappaport, S. A., & Breton, R. P. 2010, ApJ, 715, 51
Wiktorowicz, G., Middleton, M., Khan, N., et al. 2021, MNRAS, 507, 374
Witt, H. J., & Mao, S. 1994, ApJ, 430, 505